He^+ Lamb-shift measurement by the quenching-radiation anisotropy method

G. W. F. Drake, S. P. Goldman, and A. van Wijngaarden
Department of Physics, University of Windsor, Windsor, Ontario N9B 3P4, Canada
(Received 20 April 1979)

The Lamb shift of He^+ is derived from the measured anisotropy in the electric-field-induced quenching radiation of the metastable $2s_{1/2}$ state. The results demonstrate that the anisotropy method can be applied with high precision to one-electron ion beams, as well as neutral beams. We find a Lamb shift of 14040.2 ± 2.9 MHz (1 standard deviation). The sources of error and difficulties encountered in working with ion beams are discussed in detail.

I. INTRODUCTION

The precise measurement of Lamb shifts in heavy hydrogenic ions remains a significant challenge in experimental physics. Such measurements are motivated by the need to test the computational techniques of quantum electrodynamics. The methods of Erickson[1] and of Mohr[2] for calculating the higher-order (in αZ) binding-energy corrections to the electron self-energy part lead to percentage differences in the predicted Lamb shift which increase approximately as Z^2 along the isoelectronic sequence. For example, the theoretical differences increase from 0.004% for H to 0.4% for O^{7+}. If the experimental accuracy for H (± 0.002%) (Ref. 3) could be achieved in the heavier hydrogenic ions, the predictions of the current theories could be clearly separated. Unfortunately, experimental errors in previously published data also increase approximately as Z^2 so that ratios of experimental to theoretical uncertainties remain about constant. A number of measurements on ions up to $Z = 9$ are reviewed by Kugel and Murnick.[4] Since then, Gould and Marrus[5] have published the most significant heavy-ion measurement to date (in terms of distinguishing different theories) for hydrogenic argon ($Z = 18$). Even here, their uncertainty of ±1.6% is just barely sufficient to favor Mohr's calculation of the Lamb shift over Erickson's. Their experimental value is 38.0 ± 0.6 THz, while the two theoretical values are 38.25 ± 0.025 THz and 39.0 ± 0.16 THz, respectively.

In a previous sequence of papers,[6-9] we have developed the anisotropy method as an alternative way of measuring the Lamb shift. The method is based on the observation that when a hydrogenic atom in the metastable $2s_{1/2}$ state is quenched by an electric field, the induced Lyman-α (Ly-α) radiation intensity possesses an anisotropy in its angular distribution which is (nearly) proportional to the Lamb shift. The ratio $I_\parallel / I_\perp$ of the intensities emitted parallel and perpendicular to the applied electric field direction is measured. The corresponding anisotropy $R = (I_\parallel - I_\perp)/(I_\parallel + I_\perp)$ is a maximum for these two directions. R can be measured at a single point along the beam with high precision by photon counting techniques.

In Ref. 8 we have demonstrated that an accuracy of ±0.0014% (140 ppm) in the Lamb shift can be obtained for deuterium by the anisotropy method. The dominant source of error was the statistical uncertainty in the limited number of photon counts recorded in the experiment. In this paper we extend the measurements to He^+ in order to investigate what additional problems might arise in working with ion beams.

Since the apparatus and methods of analysis are basically the same as in Ref. 8, these points are only briefly summarized in the following sections, with the emphasis being on the ways in which the present work differs from our previous work. The results are nearly as accurate as the two previous measurements of the Lamb shift in He^+ by microwave resonance techniques.[10,11]

II. APPARATUS AND PROCEDURE

A. 2.1 Overall Plan

The apparatus shown in Fig. 1 is basically the same as that described previously,[8] but modifications have been made to the gas cell, the prequenching region and the photon detection system. The overall plan of the experiment is as follows. A He^+-ion beam containing a large fraction of metastables is formed by passing a beam of 90-keV ground-state He^+ ions through a gas cell. The emergent beam is collimated and then enters the quadrupole field region. Here, the induced photons emitted in two perpendicular directions are counted simultaneously by a double counter system. Counting times are normalized by monitoring the beam with a Faraday cup. All data were taken at a single quenching field strength of 599.4 V/cm at the center of the observation region.

 © 1979 The American Physical Society

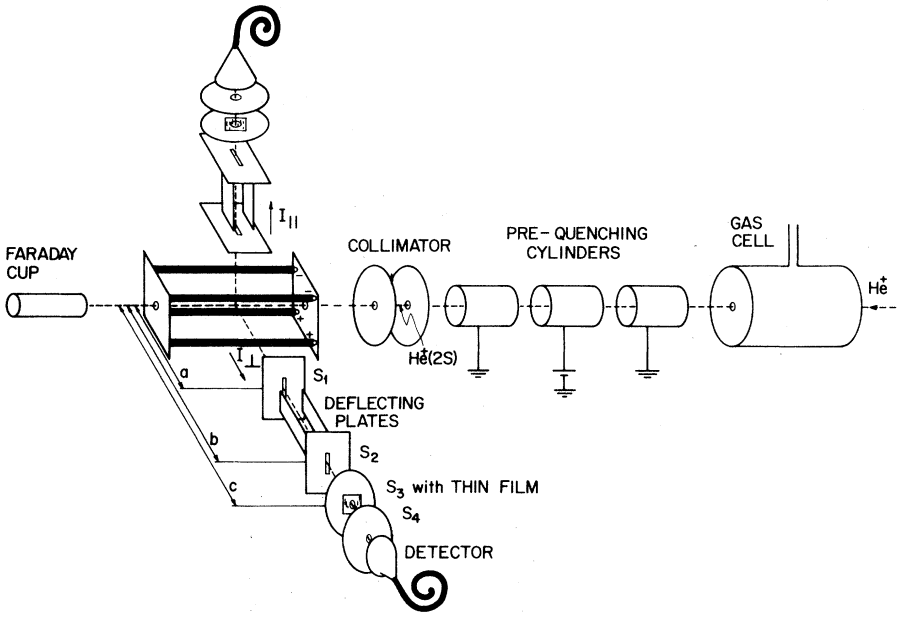

FIG. 1. Schematic diagram of the apparatus with details of the photon counting system. The slits S_1 and S_2 are mounted at distances $a = 4.83$ cm and $b = 10.92$ cm from the beam axis.

B. Gas Cell and Metastable Yield

As the gas pressure in the differentially pumped gas cell is increased, the metastable content of the emerging beam first increases, reaches a maximum, and then decreases. The maximum yield was measured for target gases of He, N_2, and Ar in the energy range 50–90 keV. The yield increases rapidly with energy, and is highest for He—a factor of 4 larger than for Ar. The signal-to-noise ratio for the quench radiation has a similiar energy dependence and reaches a saturation level near 90 keV.

C. Photon Detection and Noise

A major difficulty in this experiment arises from the many charged particles and metastable ions produced by the fast He^+ beam as it passes through the residual gas in the quenching cell. The charged particles are accelerated by the quenching field, and if they were allowed to enter the open cones of the channeltron photon detectors, the noise produced would not only be excessively large, but the magnitude would depend on the direction of the quenching field to produce a false anisotropy. The photon detection system has therefore been designed to filter out charged particles so that only the 300-Å Ly-α quench radiation is detected.

The elements of the filter system shown in Fig. 1 are as follows. The quench radiation passes through slit S_1(0.737 cm× 0.381 cm), slit S_2(0.737 cm× 0.445 cm), a circular defining slit S_3(0.559 cm diameter), a shield S_4 with a circular opening, and then enters the channeltron. The slit S_3 is covered with a thin Formvar window. The purpose of S_4 is to shield the channeltron cone from stray electric fields which originate from static charges on the insulating window. The films were prepared by the method of Revell and Agar[12] and should, accordingly, have a thickness of a few hundred angstroms. Self-supporting windows of smaller thickness are too fragile and could not be made without pin holes.

When the quench radiation was observed without windows, the background noise was as much as 50% of the signal for large quenching fields. A deflecting electric field in front of the channeltron reduced the noise somewhat, but not sufficiently. The Formvar windows, however, attenuated the background relative to the signal by about two orders of magnitude, while reducing the Ly-α signal by a factor of 2 to 3, depending on the film thickness. Despite the large reduction in noise, the windows apparently did not stop the most energetic of the charged particles. These were deflected by a transverse field of 500 V/cm (D in Fig. 1), thereby reducing the noise by a further factor of 2.

The remaining noise (~ 1% of the signal) was measured by observing the residual quenching signal under identical conditions, except that the metastables were removed from the beam by application of the axial prequenching field (see Fig. 1). This noise exhibits a small anisotropy similar to the signal itself. The anisotropy is due to the quenching of a few metastables which are regenerated by collisions of the He^+ beam with the background gas. Cascades from higher He^+ states

were suppressed by the long time delay of about 1 μsec between excitation in the gas cell and arrival at the observation region. Other possible sources of anisotropic radiation, such as excitation in the quenching cell of the background gas or short-lived He^+ states, would lead in general to an anomalous pressure dependence of the noise. Assuming the theoretical value for R, we have verified that the anisotropic part of the noise is, in fact, proportional to the background gas pressure in the range 5×10^{-8}–5×10^{-7} Torr. A small fraction of neutral helium metastables may be present, but these are not significantly quenched by fields as small as 500 V/cm. The *true* noise is therefore defined to be the isotropic part of the residual signal.

D. Limitations of Photon Detectors

As shown in Sec. IV the precision of the present results is limited primarily by photon counting statistics. The precision could, in principle, be improved by counting longer. However, the limited useful lifetime of the Galileo Optics channeltrons proved to be a serious problem. After a few times 10^8 counts, the channeltrons became nonlinear—the quantum efficiency increasing slightly with increasing count rate. The onset of the effect in time is rather sharp, and is evident in the data as an apparent increase in the anisotropy. As one check, we observed whether the anisotropy was independent of the channeltron accelerating potential over a range of a few hundred volts about its plateau. The check was carried out before and after sequences of about 40 measurements, each one containing about 10^6 counts. If a consistent discrepancy was found, the entire sequence was rejected and new channeltrons installed. In this way, three different pairs of channeltrons were used in collecting the present data.

We also experimented with ceramic channeltrons (Murata Co.). These have a useful lifetime of linearity which is at least three times longer than the Galileo Optics channeltrons, but the quantum efficiency is an order of magnitude smaller. The quantum efficiency can be restored and the longer lifetime preserved by placing the cones from Galileo Optics channeltrons in front of the Murata channeltrons in such a way that the latter detects the photoelectron pulses from the former. Because of a long testing period, only a small amount of useful data was actually obtained in this way before loss of linearity.

III. THEORY

As in Ref. 8, R is calculated as a function of the Lamb shift, and then the Lamb shift is deduced from the measured value of R. The calculation of R for $^4He^+$ is much simpler than for D owing to the absence of hyperfine structure. In general, different hyperfine (or Zeeman) components of the electric-field-perturbed $2s_{1/2}$ state are quenched at different rates, with the result that R is weakly time dependent in the observation region. Since there is no magnetic field or hyperfine structure in the present work, R is time independent (except for rapidly decaying transient effects associated with beam entry into the dc field region).

The detailed method of calculation is described in Ref. 8. However, the results for the present simple case are easily understood by the following argument. Taking the z axis as the dc field axis, the adiabatic field-perturbed initial state is

$$\psi_i = \frac{1}{N^{1/2}}\left[\psi(2s_{1/2}) + \alpha\psi(2p_{1/2}) + \sqrt{2}\,\beta\psi(2p_{3/2})\right], \tag{1}$$

where α and $\sqrt{2}\beta$ are mixing coefficients determined by diagonalizing the complete Hamiltonian, including the external field, in the $2s_{1/2}$, $2p_{1/2}$, $2p_{3/2}$ basis set, and N is a normalization constant. Defining ρ by

$$\rho = \beta/\alpha\ , \tag{2}$$

then in the limit of weak fields

$$\rho = \frac{E(2s_{1/2}) - E(2p_{1/2}) + \frac{1}{2}i\Gamma_p}{E(2s_{1/2}) - E(2p_{3/2}) + \frac{1}{2}i\Gamma_p}\ . \tag{3}$$

In the electric dipole approximation, the emitted radiation intensity with polarization vector $\hat{e}$ is proportional to

$$I(\hat{e}) = |\langle\psi_i|\,\hat{e}\cdot\vec{r}\,|1s_{1/2}\rangle|^2\ . \tag{4}$$

The radiation emitted in a given direction is obtained by summing (4) over two perpendicular $\hat{e}$ vectors, both perpendicular to the direction of propagation. Evaluating the matrix elements in (4) yields

$$I(\theta) \propto |\alpha|^2\left[1 + \mathrm{Re}(\rho)(1 - 3\cos^2\theta) + |\rho|^2\left(\tfrac{5}{2} - \tfrac{3}{2}\cos^2\theta\right)\right] \tag{5}$$

for the intensity per unit solid angle emitted at an angle θ from the z axis. The anisotropy is therefore

$$R_0 = \left[I(0) - I(\tfrac{1}{2}\pi)\right]/\left[I(0) + I(\tfrac{1}{2}\pi)\right]$$

$$= \left[-3\,\mathrm{Re}(\rho) - \tfrac{3}{2}|\rho|^2\right]/\left[2 - \mathrm{Re}(\rho) + \tfrac{7}{2}|\rho|^2\right]\ . \tag{6}$$

The above formula emphasizes that $R \simeq -3/2\,\mathrm{Re}(\rho)$ is determined primarily by the ratio of the Lamb shift to the fine-structure splitting.

TABLE I. Input data (x) for theoretical calculation of the He^+ anisotropy (R) and sensitivity coefficients (s).[a]

x	Value	s
$E(2s_{1/2}-2p_{1/2})$	14042.05 MHz	0.97
$E(2p_{3/2}-2p_{1/2})$	161552.0 MHz	−0.97
$\Gamma(2p)$	1.002×10^{10} sec^{-1}	−0.0005
Field strength	599.4 V/cm	0.004

[a]The coefficient s is defined by $\delta R/R = s\,\delta x/x$, where δR is the change in R induced by a change δx in x.

The actual calculations of R were done by solving exactly the nonrelativistic time-dependent Schrödinger equation in the subset of states with $n=2$ as described in Ref. 8, using the input data in Table I. The results in this approximation are well represented by the truncated expansion

$$R_0 = R^{(0)} + R^{(2)}\epsilon^2 + R^{(4)}\epsilon^4 , \tag{7}$$

where ϵ is the dc field strength in kV/cm. The leading term of (7) is given exactly by (6). The coefficients $R^{(n)}$ are listed for several ions in Table II. For He^+, Eq. (7) is accurate to ~1 ppm for $\epsilon \lesssim 1$ kV/cm. However, contributions from intermediate p states with $n>2$, final-state perturbations, and relativistic effects all contribute small corrections as discussed in Sec. III A.

An expansion of the form (7) is only useful for ions with zero nuclear spin. For nonzero nuclear spin, the perturbation expansion underlying (7) applies only if the Stark shifts are small compared with the hyperfine-structure splittings. In addition, R becomes weakly time dependent owing to the different depopulation rates of different hyperfine states.

A. Small Corrections

We consider first the contributions from intermediate p states with $n>2$ and final-state perturbations in the nonrelativistic limit. This is followed by a discussion of relativistic and retardation effects.

The contributions from intermediate p states with $n>2$, and perturbation corrections to the $1s_{1/2}$ final state, are both included in the calculations of Ref. 9, where static field quenching is regarded as the zero-frequency limit of a two-photon process. The corrections are calculated in terms of the parameters B and C defined by

$$B = \sum_{n>2}^{\infty} \frac{\langle 2s|z|np\rangle\langle np|z|1s\rangle}{E(2s)-E(np)} , \tag{8}$$

$$C = \sum_{n=2}^{\infty} \frac{\langle 2s|z|np\rangle\langle np|z|1s\rangle}{E(1s)-E(np)} . \tag{9}$$

B represents the contribution from virtual transitions through high np states, and C the contribution from final-state perturbations. Using the analysis of Ref. 9 and neglecting the level widths, the fractional correction to R_0 in the limit of weak fields can be shown to be

$$\left(\frac{\delta R}{R_0}\right)_{B+C} = 2(B+C)\frac{\Delta E_F}{M}\left(\frac{1+2\rho}{2+\rho}\right)(1+R_0) , \tag{10}$$

where

$$\Delta E_F = E(2s_{1/2}) - E(2p_{3/2}) ,$$

$$M = \langle 1s|z|2p\rangle\langle 2p|z|2s\rangle .$$

Using the values[9]

$B = 12.416\,Z^{-4}$ a.u., $C = -3.476\,Z^{-4}$ a.u., and $M = (-2^7\sqrt{2}/81)Z^{-2}$ a.u., and expressing ΔE_F in a.u., then

$$(\delta R/R_0)_{B+C} = 8.00\frac{\Delta E_F}{Z^2}\left(\frac{1+2\rho}{2+\rho}\right)(1+R_0) \tag{11}$$

to better than 0.1% accuracy. The numerical values of (11) are approximately $-6\times10^{-6}Z^2$ for all $Z \lesssim 20$. The precise value for He^+ is -23.7×10^{-6}. The errors introduced by neglecting the level widths and field-dependent corrections to (11) introduce errors in R of less than 1 ppm for He^+ and are therefore negligible.

The lowest-order relativistic corrections to R are just the relativistic and retardation corrections of order α^2Z^2 to the electric dipole radiation and external-field matrix elements. The calculations of these corrections is described in Ref. 7. Again neglecting level-width and field-dependent corrections, the fractional change in R_0 due to

TABLE II. Data for calculating the anisotropy of ions with zero nuclear spin [see Eq. (14)].

Ion	$R^{(0)}$	$R^{(2)}$ [a]	$(\delta R/R)_{B+C}$	$(\delta R/R)_{\rm rel}$	$(\delta R/R)_{M2}$
He^+	0.117 965 6	5.822 (−4)	−2.37(−5)	0.644(−5)	−6.54(−5)
C^{5+}	0.081 718 2	1.557 (−8)	−2.23(−4)	0.608(−4)	−5.71(−4)
O^{7+}	0.072 662 0	1.000 (−9)	−4.02(−4)	1.091(−4)	−10.09(−4)
Ne^{9+}	0.065 864 9	1.194(−10)	−6.33(−4)	1.716(−4)	−15.7 (−4)

[a] For He^+, $R^{(4)} = -0.37\times10^{-5}$.

relativistic effects is

$$\left(\frac{\delta R}{R_0}\right)_{\rm rel} = \frac{(\mu_3+\mu_3'-\mu_1-\mu_1')(1-\rho)(1+2\rho)}{(1+\frac{1}{2}\rho)(1-\frac{1}{2}\rho+\frac{7}{4}\rho^2)}\,, \qquad (12)$$

where μ_3, μ_3', μ_1, and μ_1' are the fractional changes due to relativistic effects in the matrix elements $\langle 2s_{1/2}|z|2p_{3/2}\rangle$, $\langle 2p_{3/2}|\vec{\alpha}\cdot\vec{A}|1s_{1/2}\rangle$, $\langle 2s_{1/2}|z|2p_{1/2}\rangle$, and $\langle 2p_{1/2}|\vec{\alpha}\cdot\vec{A}|1s_{1/2}\rangle$, respectively. Here ez is the external-electric-field operator and $\vec{\alpha}\cdot\vec{A}$ is the usual Dirac form of the radiation-interaction operator for electric dipole transitions. Using the values

$$\mu_3 = -\tfrac{1}{6}\alpha^2Z^2, \quad \mu_1 = -\tfrac{5}{12}\alpha^2Z^2\,,$$

$$\mu_3' = (-\tfrac{11}{48} - \tfrac{5}{4}\ln 2 + \tfrac{3}{4}\ln 3)\alpha^2Z^2\,,$$

$$\mu_1' = (-\tfrac{11}{96} - \tfrac{3}{2}\ln 2 + \ln 3)\alpha^2Z^2\,,$$

the correction (12) is roughly $1.7\times10^{-6}\,Z^2$ for $Z \lesssim 20$. The precise value for He^+ is 6.4×10^{-6}.

Recently, Hillery and Mohr[13] have shown that the interference term between the electric field induced $2s_{1/2}-2p_{1/2}-1s_{1/2}$ electric dipole (E1) and $2s_{1/2}-2p_{3/2}-1s_{1/2}$ magnetic quadrupole (M2) decay modes introduces an additional correction of relative order α^2Z^2 to R. Using their results in lowest order, the additional correction is

$$\left(\frac{\delta R}{R_0}\right)_{\rm M2} = -\mu_{\rm M2}\frac{(1-\rho)(1-\frac{1}{3}R_0)}{(1+\frac{1}{2}\rho)} \qquad (13)$$

with $\mu_{\rm M2}=9\alpha^2Z^2/32$. The correction is approximately $-16\times10^{-6}Z^2$, and the precise value for He^+ is -65.4×10^{-6}. Combining (7) with (11), (12), and (13) yields the final theoretical expression for the anisotropy

$$R_T = R^{(0)}\left[1+\left(\frac{\delta R}{R_0}\right)_{B+C}+\left(\frac{\delta R}{R_0}\right)_{\rm rel}+\left(\frac{\delta R}{R_0}\right)_{\rm M2}\right] + R^{(2)}\epsilon^2 + R^{(4)}\epsilon^4\,. \qquad (14)$$

Further small rotational asymmetries resulting from interference terms with the spontaneous $2s_{1/2}-1s_{1/2}$ M1 decay mode have recently been discussed.[14,15] However, these cancel out in lowest order if the intensities in directions $\vec{k}$ and $-\vec{k}$ are combined to form the geometric mean as described previously.[6]

IV. EXPERIMENTAL DATA AND STATISTICAL ANALYSIS

In all, 1450 individual measurements of R were made, each measurement containing on the average 1.225×10^6 counts for a total of 1.7755×10^9 counts. The data were obtained in 20 separate runs made on different days. Each complete measurement of R was assembled from eight separate counter readings—one for each of the two counters at the four electric field directions obtained by switching the potentials on the quadrupole rods (see Fig. 1). The data were combined in ratios in such a way that the relative sensitivities of the two counter systems were eliminated.[6]

The mean and standard deviation of all the measurements weighted by the number of counts in each measurement, are defined by

$$\bar{R} = \sum_{i=1}^{N}\frac{R_i n_i}{n_T} \qquad (15)$$

and

$$\sigma = \left(\sum_{i=1}^{N}\frac{(R_i-\bar{R})^2 n_i}{n_T(N-1)}\right)^{1/2}\,, \qquad (16)$$

where n_i is the number of counts in the ith measurement, n_T is the total number of counts, and

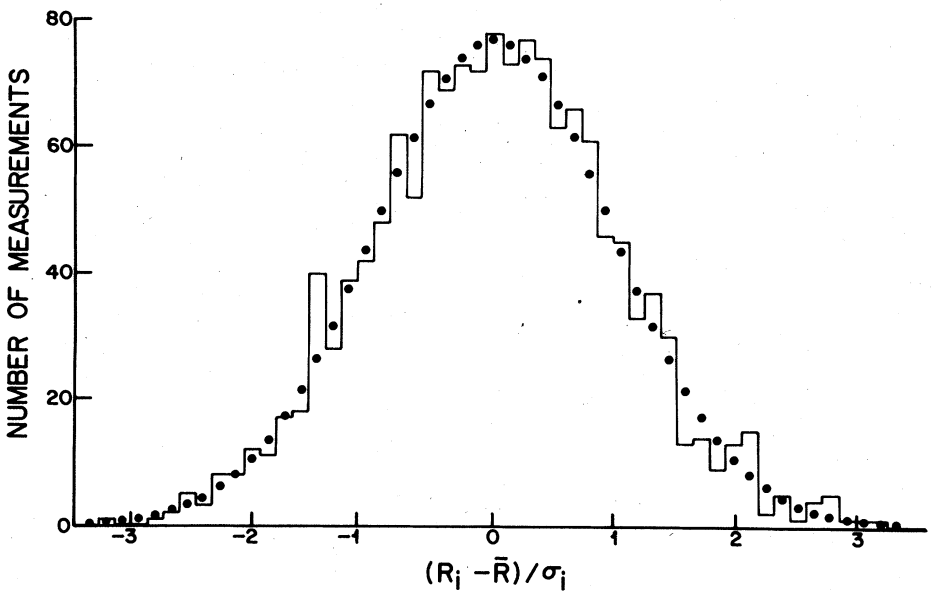

FIG. 2. Histogram for the distribution of the experimental data about the mean in units of the expected standard deviation for each point. The solid circles show the expected bar heights for a Gaussian distribution with the same mean and unit half-width.

N is the number of measurements. The experimental values are

$$\bar{R} = 0.118\,0726, \quad \sigma = 0.000\,0244$$

uncorrected for the finite solid angle of observation, beam bending by the quenching field, and electronic dead time. The theoretically expected standard deviation arising from counting statistics for both the signal and noise is

$$\sigma_{\rm tot} = (\sigma_R^2 + \sigma_{\rm noise}^2)^{1/2}, \tag{17}$$

where

$$\sigma_R = \tfrac{1}{2}(\alpha^{1/2} + \alpha^{-1/2})[(1-R^2)/n_T]^{1/2} \tag{18}$$

$$\sigma_{\rm noise} = \sigma_R F \left(\frac{R_{\rm noise}}{n_T}\right)^{1/2} \left(\frac{1+R^2}{1-R^2}\right)^{1/2}, \tag{19}$$

α is the ratio of the sensitivities of the two-counter systems, F is the number of signal measurements between each noise measurement, and $n_{\rm noise}/n_T$ is the noise-to-signal ratio. In the present series of measurements, it was necessary to take into account changes in α from one run to the next, together with slow drifts in α in the course of a given measurement. When this is done, the predicted standard deviation is

$$\sigma_{\rm tot} = 0.000\,0243$$

in satisfactory agreement with the experimental value. It is satisfying that despite repeated replacements of the channeltrons and possible errors from nonlinearity in their response, the fluctuations in the data are no worse than what can be accounted for by counting statistics alone. We also compare in Fig. 2 the histogram of the experimental data distribution about the mean (in units of the expected standard deviation for each point) with the theoretically expected histogram for a Gaussian distribution with unit standard deviation. The χ^2 test of the fit with the mean as the only adjustable parameter, yields $\chi^2 = 24.7$ for 36 degrees of freedom. One could expect a worse fit about 90% of the time. The results of the runs tests[8, 10] are given in Table III. None of these tests reveals statistically significant anomalies in the data.

TABLE III. Comparison of the observed numbers of low and high runs with the expected number of runs.

Run length	Low runs	High runs	Expected number
1	186	189	181 ± 12
2	87	80	91 ± 9
3	46	47	45 ± 6
4	25	26	23 ± 4
5	10	19	11 ± 3
6	8	1	5.7 ± 2.3
7	1	3	2.8 ± 1.6
8	0	0	1.4 ± 1.1
9	0	0	0.7 ± 0.8
10	1	1	0.35 ± 0.58
11	1	0	0.18 ± 0.42
Total	365	366	362.5 ± 9.5

TABLE IV. Systematic corrections to the observed anisotropy.

Correction	$\delta R/R$ (ppm)
Solid angle	617
Dead time	73
Beam bending	−34
Total	656

The experimental value for R must still be corrected for three systematic effects—the finite angle of observation, electronic dead time, and the bending of the He^+ beam by the quenching field. The first two have been discussed in Ref. 8, while the third is a new effect not present for neutral beams. Beam bending alters the apparent anisotropy because (1) the distances to the counters are changed and (2) the angles of observation with respect to the quenching-field direction are changed. The first effect increases the observed anisotropy because the apparent intensity of a line source is proportional to D^{-1}, where D is the perpendicular distance from the beam to the counter. The second effect tends to decrease the observed anisotropy. For a small deflection δ, and $\epsilon = \delta/D$, the fractional corrections to the observed value of R due to (1) and (2) are

$$\left(\frac{\delta R}{R}\right)_{\rm bending} = -\frac{\epsilon^2}{2R}(1-R^2) + \epsilon^2(1+R), \tag{20}$$

respectively. For our field strength and geometry, the calculated value of ϵ is 0.003 34, giving a fractional correction to the observed value of R of -3.39×10^{-5}. The values for the other systematic corrections to R are summarized in Table IV. Combining all of these gives the final experimental value

$$R_{\rm exp} = 0.118\,150 \pm 0.000\,024$$

(one standard deviation) in agreement with the theoretical value 0.118 164 derived from the input

TABLE V. Sources of error in the measurement of R due to uncertainties in various parameters.

Parameter	$\delta R/R$ (ppm)
Counting statistics	204
Dead-time correction	10
Solid angle correction	5
Electric field strength	3
Beam-bending correction	3
$(\sum_i \delta R_i^2)^{1/2}/R$	204

TABLE VI. Comparison of experimental and theoretical Lamb shifts for He^+ (in MHz).

Experiment	Theory
14 040.2 ± 2.9 [a]	14 042.05 ± 0.55 [d]
14 040.2 ± 1.8 [b]	14 044.78 ± 0.61 [e]
14 046.2 ± 1.2 [c]	

[a] Present work.
[b] Lipworth and Novick (Ref. 10).
[c] Narasimham and Strombotne (Ref. 11).
[d] Mohr (Ref. 2).
[e] Erickson (Ref. 1).

data in Table I and Eq. (13). The various sources of experimental uncertainty are listed in Table V. It is clear that the uncertainty arising from counting statistics is by far the dominant source of error.

V. RESULTS AND DISCUSSION

Our experimental value for R corresponds to a Lamb shift of 140 40.2 ± 2.9 MHz. This is compared with other experimental and theoretical values in Table VI. Our Lamb shift is in satisfactory agreement with the earlier measurement of Lipworth and Novick[10] and the recent calculation of Mohr,[2] but lies significantly below the measurement of Narasimham and Strombotne,[11] and the calculation of Erickson.[1] Our conclusions regarding agreement with the two theoretical values is in harmony with that of Gould and Marrus[5] for Ar^{17+}.

The theoretical and experimental Lamb shifts are compared in Fig. 3 for a number of ions from H to Ar^{17+}. The results are expressed as the deviation from the average of Erickson's and Mohr's theoretical values, divided by Z^6. Except for the anisotropy measurements for D and He^+, and the recent quench rate measurement[5] for Ar^{17+}, the data are the same as tabulated by Kugel and Murnick.[4] The scaling factor of Z^{-6} reduces all the theoretical deviations and experimental error bars to about the same size. The figure emphasizes that little has yet been gained by going to heavy ions in terms of distinguishing between the two theories. All the data taken together do not appear to favor one theory over the other.

The accuracy of the present experiment could be considerably improved by increasing the number of photon counts recorded. The statistical uncertainty in the photon counting rate accounts for nearly all of the uncertainty in our final result. However, it does not appear to be feasible to

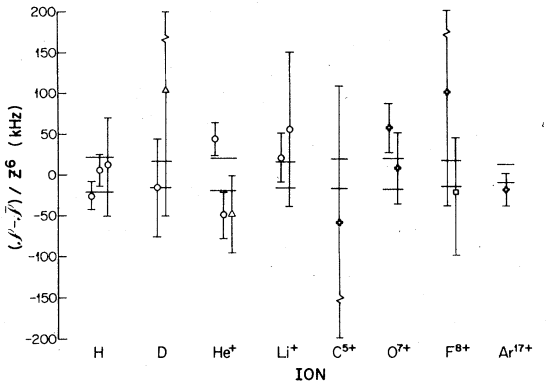

FIG. 3. Comparison between scaled theoretical and experimental Lamb shifts, expressed as deviations from the theoretical mean. The upper horizontal line is Erickson's theory, the lower horizontal line is Mohr's theory and $\bar{S}$ is the average of the two. The experimental data are labeled by method of measurement according to ○, microwave resonance; △, anisotropy measurement; +, quench rate measurement; □, laser resonance.

attempt a significant improvement in accuracy until a way has been found to avoid the small nonlinearities which develop in the response of the channeltrons as they age (see Sec. IID). The one other systematic effect which is difficult to eliminate with certainty is a possible asymmetry in the background noise due to the acceleration of charged particles by the quenching field into the parallel detector (see Sec. IIC). It is significant that both these effects, if present, would tend to increase the measured anisotropy (and hence Lamb shift) above its true value. We took great care to reduce these effects to a negligible level, but an unsuspected further correction for them would reduce our already low value for the Lamb shift still further.

This work demonstrates that the anisotropy method for measuring the Lamb shift can be applied with high precision to a hydrogenic ion beam. The results suggest that a similar measurement for a heavier hydrogenic ion would be well worth attemping as a definitive test of computational methods for the Lamb shift.

ACKNOWLEDGMENT

Support by the Natural Sciences and Engineering Research Council of Canada is gratefully acknowledged.

[1]G. W. Erickson, Phys. Rev. Lett. 27, 780 (1971); J. Phys. Chem. Ref. Data 6, 831 (1977).
[2]P. J. Mohr, Phys. Rev. Lett. 34, 1050 (1975); Ann. Phys. (N.Y.) 88, 26 (1974); in *Beam-Foil Spectroscopy*, edited by I. A. Sellin and D. J. Pegg (Plenum, New York, 1976), p. 89.
[3]S. R. Lundeen and F. M. Pipkin, Phys. Rev. Lett. 34, 1368 (1975); D. A. Andrews and G. Newton, *ibid.* 37, 1254 (1976).
[4]H. W. Kugel and D. E. Marnick, Rep. Prog. Phys. 40, 297 (1977).
[5]H. Gould and R. Marrus, Phys. Rev. Lett. 41, 1457 (1978).
[6]G. W. F. Drake, P. S. Farago, and A. van Wijngaarden, Phys. Rev. A 11, 1621 (1975).
[7]G. W. F. Drake and C-P. Lin, Phys. Rev. A 14, 1296 (1976).
[8]A. van Wijngaarden and G. W. F. Drake, Phys. Rev. A 17, 1366 (1978).
[9]G. W. F. Drake and R. B. Grimley, Phys. Rev. A 8, 157 (1973).
[10]E. Lipworth and R. Novick, Phys. Rev. 108, 1434 (1957)
[11]M. Narasimham and R. Strombotne, Phys. Rev. A 4, 14 (1971).
[12]R. S. M. Revell and A. W. Agar, Brit. J. Appl. Phys. 6, 23 (1955).
[13]Mark Hillery and Peter J. Mohr, Phys. Rev. A (to be published).
[14]P. J. Mohr, Phys. Rev. Lett. 40, 854 (1978).
[15]G. W. F. Drake, Phys. Rev. Lett. 40, 1705 (1978).